(12) INTERNATIONAL APPLICATION PUBLISHED UNDER THE PATENT COOPERATION TREATY (PCT)

(19) World Intellectual Property Organization
International Bureau

(43) International Publication Date
29 December 2011 (29.12.2011)

PCT

(10) International Publication Number
WO 2011/162849 A2

(51) International Patent Classification:
F28F 13/00 (2006.01) *B82B 1/00* (2006.01)
F28F 1/10 (2006.01) *F28F 13/02* (2006.01)

(21) International Application Number:
PCT/US2011/031008

(22) International Filing Date:
1 April 2011 (01.04.2011)

(25) Filing Language: English

(26) Publication Language: English

(30) Priority Data:
61/320,248 1 April 2010 (01.04.2010) US
61/470,999 1 April 2011 (01.04.2011) US

(71) Applicant *(for all designated States except US)*: **THE BOARD OF REGENTS OF THE NEVADA SYSTEM OF HIGHER EDUCATION, on behalf of THE UNIVERSITY OF NEVADA, RENO** [US/US]; 1664 N. Virginia Street, Reno, NV 89557 (US).

(72) Inventor; and
(75) Inventor/Applicant *(for US only)*: **PARK, Chanwoo** [US/US]; 11135 Messina Way, Reno, NV 89521 (US).

(74) Agent: **BRADLEY, Karri, Kuenzli**; Klarquist Sparkman, LLP, One World Trade Center, Suite 1600, 121 SW Salmon Street, Portland, OR 97204 (US).

(81) Designated States *(unless otherwise indicated, for every kind of national protection available)*: AE, AG, AL, AM, AO, AT, AU, AZ, BA, BB, BG, BH, BR, BW, BY, BZ, CA, CH, CL, CN, CO, CR, CU, CZ, DE, DK, DM, DO, DZ, EC, EE, EG, ES, FI, GB, GD, GE, GH, GM, GT, HN, HR, HU, ID, IL, IN, IS, JP, KE, KG, KM, KN, KP, KR, KZ, LA, LC, LK, LR, LS, LT, LU, LY, MA, MD, ME, MG, MK, MN, MW, MX, MY, MZ, NA, NG, NI, NO, NZ, OM, PE, PG, PH, PL, PT, RO, RS, RU, SC, SD, SE, SG, SK, SL, SM, ST, SV, SY, TH, TJ, TM, TN, TR, TT, TZ, UA, UG, US, UZ, VC, VN, ZA, ZM, ZW.

(84) Designated States *(unless otherwise indicated, for every kind of regional protection available)*: ARIPO (BW, GH, GM, KE, LR, LS, MW, MZ, NA, SD, SL, SZ, TZ, UG, ZM, ZW), Eurasian (AM, AZ, BY, KG, KZ, MD, RU, TJ, TM), European (AL, AT, BE, BG, CH, CY, CZ, DE, DK, EE, ES, FI, FR, GB, GR, HR, HU, IE, IS, IT, LT, LU, LV, MC, MK, MT, NL, NO, PL, PT, RO, RS, SE, SI, SK, SM, TR), OAPI (BF, BJ, CF, CG, CI, CM, GA, GN, GQ, GW, ML, MR, NE, SN, TD, TG).

Declarations under Rule 4.17:

— *of inventorship (Rule 4.17(iv))*

Published:

— *without international search report and to be republished upon receipt of that report (Rule 48.2(g))*

WO 2011/162849 A2

(54) **Title**: DEVICE HAVING NANO-COATED POROUS INTEGRAL FINS

(57) **Abstract**: Disclosed herein is an apparatus including a plurality of nano-coated, porous integral fins and/or grooves on the evaporator tubes. In some examples, the apparatus is an evaporative cooler, such as a horizontal-tube, falling-film evaporator. In some examples, the evaporator tubes are in either a horizontal and/or tilted and/or vertical position. Also disclosed are methods of using the disclosed apparatus, such as a cooling device including as an evaporative cooler.

DEVICE HAVING NANO-COATED POROUS INTEGRAL FINS

[1] CROSS REFERENCE TO RELATED APPLICATIONS

[2] This application claims the benefit of U.S. Provisional Application Serial No. 61/320,248, filed April 1, 2010 and U.S. Provisional Application Serial No. 61/470,999 filed April 1, 2011, each of which are incorporated by reference herein in their entirety.

[3] TECHNICAL FIELD

[4] The present disclosure relates to evaporators, such as falling-film evaporators.

[5] ACKOWLEDGMENT OF GOVERNMENT SUPPORT

[6] This invention was made with U.S. Government support of Grant No. DE-EE0003231 from the Department of Energy. The U.S. Government has certain rights in this invention.

[7] BACKGROUND

[8] Falling-film, horizontal-tube evaporators have been widely used in air-conditioning, refrigeration, chemical, petroleum refining and desalination industries. It is known that the falling-film evaporators have several advantages over flooded evaporators: (1) higher heat transfer coefficients due to jet impingement on the horizontal tubes, (2) relatively thin film evaporation (i.e., low thermal resistances resulting in high evaporator temperatures and thermodynamic cycle efficiencies and compact/lightweight design), and (3) low refrigerant (evaporant) charge and less risk associated with a leak. Despite the superior performance of the falling-film evaporators, problems associated with liquid maldistribution, surface nonwetting,

and droplet (localized and relatively thick liquid layer) formation on the plain evaporator tubes make the conventional falling-film evaporator less efficient in terms of evaporator surface utilization and thin-film (low thermal resistance) formation.

[9] Some prior work with falling-film evaporation enhancement has employed various structured surfaces, such as extended solid fins, grooves, hydrophilic coating and reentrant nucleation cavities, to enhance the evaporation performance. "Circumferential micro-grooves" on horizontal-tube evaporators "partially-immersed in liquid pools" were used to create a capillary-assisted liquid distribution within the solid grooves, thus promoting thin film evaporation. Because liquid pools were used to supply liquid over the entire length of the evaporator tubes, the liquid dispenser design creates undesirable design limitations/constraints, such as requiring multiple liquid dispensers and large tube spacing. Because of the circumferential grooves, the liquid distribution is typically allowed only in circumference of the grooves, not in the axial direction of the tube.

[10] Surface evaporation using porous-layer coating groove for a liquid pool was "numerically" analyzed. Some results indicated that evaporation can be increased in the *thin* liquid film region near liquid menisci and that capillary-assisted liquid distribution in a porous coating on triangular grooves can increase evaporation (wetting) area. Heat pipes used for commercial electronic cooling utilize the same capillary pumping for liquid circulation and thin-film nucleate boiling in the porous wicks. Note that the capillary pumping can typically self-regulate itself to varying heat loads, thus forming a thin liquid film within the porous layer. The capillary

pumping is generally inversely proportional to the pore diameter of the porous wicks.

[11] Pool boiling enhancement using porous-layer coatings with surface modulations (periodically non-uniform thickness) and laminated screen meshes has been studied by some researchers. Generally, the results indicate that the pool-boiling Critical Heat Flux (CHF) using surface modulations was increased nearly three times over that of a plain surface because the modulation separates the liquid and vapor streams, thus reducing the liquid-vapor counterflow resistances adjacent to the surface and improving the hydrodynamic stability in the vapor-liquid interface, thus increasing the pool boiling CHF.

[12] It has been known that surface roughness and oxidation (aging) can alter pool boiling characteristics, such as because of the increased nucleation sites and improved surface wetting and because surface oxidation can introduce a nano-scale surface morphology to the original surfaces, and increases surface wettability. Although metal oxides (e.g., CuO and Al_2O_3) have lower thermal conductivities than original metals resulting in higher conduction resistances, increased nucleation sites (new nano-scale surface morphology) and surface wettability (hydrophilicity) of the oxide surfaces can significantly alter liquid distribution and surface wetting characteristics and improve the overall boiling performance.

[13] In other studies, the effect of degree of oxidation of the heater surface on nucleate *pool* boiling and the surface oxidation was quantitatively measured by static contact angle of a sessile water drop. This study attempted to correlate the surface oxidation to wettability (contact angle) and pool boiling heat flux. It was reported

that as the surface wettability improves by the surface oxidation, the maximum heat flux increases and a higher surperheat is required to attain the same heat flux.

[14] In further studies, it was found that the influence of the surface roughness is small for the fully-developed film boiling where vapor film thicknesses are considerably larger than wall roughness. But as the vapor film gets thinner near the pool-boiling minimum heat flux condition, the surface roughness elements could interact with the liquid-vapor interface and the boiling curve could be significantly altered. The surface oxidation was reported to increases the pool-boiling minimum heat flux where the oxide surface (hydrophilic) easily spreads the liquid as the liquid contact begins to occur. As the pool-boiling CHF is approached, the influence of surface roughness wanes because the CHF is thought to depend primarily on the hydrodynamics of vapor removal and gets stronger on the nucleate boiling portion of the boiling curves.

[15] Surface nano-coating was used to influence surface wettability from *hydrophilicity* (SiO_x, TiO_2,, Pt and Fe_2O_3) to *hydrophobicity* (SiOC and Teflon) in a further study. Particles of very small size (less than 100nm) called "nanoparticles" were deposited on the heated surface using various deposition techniques. Another recent report describes using a nanofluid with Al_2O_3 nanoparticle for the pool boiling. The study describes that the boiling critical heat flux increases compared to those of the pure fluids. The enhanced heat flux was partially attributed to increased surface wettability of the nanofluids due to the deposition of the nanoparticles on the heater surface, called Nanofluid Nucleate Boiling Deposition (NNBD).

[16] SUMMARY

[17] In one embodiment, the present disclosure provides capillary-assisted evaporation using nano-coating, porous integral fins on horizontal-tube, falling-film evaporators.

[18] In wicked heat pipes used as an electronic cooling device, capillary liquid distribution, and consequently, thin film evaporation/boiling are typically the underlying heat and mass transfer processes. According to one aspect of the present disclosure, using capillary (gravity-insensitive) liquid distribution in porous integral fins for falling-film, horizontal-tube evaporators mitigates inherent liquid maldistribution and surface nonwetting problems found in the conventional plain surface evaporators and helps approach ideal evaporation conditions, i.e., thin-film evaporation with low-thermal resistance over increased wetted surface area even with less liquid supply. In a particular implementation, nano-coating (nano-particle deposition), including oxidation on the porous fins of the falling-film evaporators, is used to further enhance surface wettability (hydrophilicity), thus increasing evaporation.

[19] In various embodiments, the present disclosure uses the following properties/variables/conditions in falling-film evaporation to improve performance: micro-structural properties (porosity, permeability, pore size(10~100μm), pore size/distribution, and specific surface area) and geometrical properties (fin height (~1cm), width and pitch), thermo-physical properties (effective thermal conductivity) of porous integral fins and surface wettability change (oxidation and nano-coating), evaporator design variables (tube diameter/length/spacing and liquid

dispenser) and operating conditions (flow rate and temperature of feed liquid and vapor pressure).

[20] There are additional features and advantages of the subject matter described herein. They will become apparent as this specification proceeds.

[21] In this regard, it is to be understood that this is a brief summary of varying aspects of the subject matter described herein. The various features described in this section, Appendix I and below for various embodiments may be used in combination or separately. Any particular embodiment need not provide all features noted above, nor solve all problems or address all issues in the prior art noted above. Additional features of the present disclosure are described in the appended claims.

[22] BRIEF DESCRIPTION OF THE DRAWINGS

[23] Various embodiments are shown and described in connection with the following drawings in which:

[24] FIG. 1A is a photograph of a thin film boiling apparatus under saturated conditions before insulation. FIG. 1B is a photograph of a sintered copper wick (porous-layer coating) showing reddish copper (I) oxide.

[25] FIGS. 2A-2B are electronic images showing the flow modes and surface wetting for falling-film water on two-row horizontal copper tubes with (a) plain surface and (b) porous-layer coating at various liquid Reynolds numbers ($\mathrm{Re}_{\mathrm{liq}} = 4\Gamma/\mu_{\mathrm{liq}}$). ζ is the surface wetting ratio defined as $\zeta = A_{\mathrm{wet}}/A_{\mathrm{tube,outer}}$.

[26] FIGS 3A-3C are digital images showing the contact angle measurement of 1 mL sessile water droplets on (a) a polished (fresh) surface (sample 1); (b) copper surface oxidized at room temperature of two days (sample 4); and (c) copper surface oxidized at 100 °C for two hours (sample 6).

[27] FIGS. 4A and 4B are diagrams illustrating a process for fabricating an integral porous fin.

[28] FIG. 5A is a schematic diagram illustrating a porous integral fin on a substrate, showing capillary-driven liquid flow/distribution and surface evaporation. FIG. 5B is a photograph of a porous integral fin built on a copper substrate. FIG. 5C is a schematic diagram illustrating a porous integral fin on a substrate. FIG. 5D is a diagram of a grooved fin.

[29] FIG. 6 is a schematic diagram of a system using a falling-film evaporator.

[30] FIG. 7 is a diagram illustrating modes of heat transfer and vapor formation in a porous layer.

[31] DETAILED DESCRIPTION

[32] Unless otherwise explained, all technical and scientific terms used herein have the same meaning as commonly understood by one of ordinary skill in the art to which this disclosure belongs. In case of conflict, the present specification, including explanations of terms, will control. The singular terms "a," "an," and "the" include plural referents unless context clearly indicates otherwise. Similarly, the word "or" is intended to include "and" unless the context clearly indicates otherwise. The term "comprising" means "including;" hence, "comprising A or B" means including A or B, as well as A and B together. Although methods and materials similar or equivalent to those described herein can be used in the practice or testing of the present disclosure, suitable methods and materials are described herein. The disclosed materials, methods, and examples are illustrative only and not intended to be limiting.

[33] In wicked heat pipes used as an electronic cooling device, capillary liquid distribution and consequently, thin film evaporation/boiling (low thermal resistance of 0.05K-cm²/W, and heat flux ≤ 200W/cm²) are typically the underlying heat and mass transfer processes. The capillary-assisted (gravity-insensitive) liquid distribution using the disclosed porous integral fins can produce enhanced cooling devices, such as falling-film, horizontal-tube evaporators, where the liquid maldistribution, poor surface wetting and liquid droplet formation inherently tends to occur. Surface oxidation (aging) is known to change pool boiling characteristics. Such changes are likely because of the increased nucleation sites and improved surface wetting associated with newly introduced nano-scale surface morphology onto the original surfaces. Although few studies exist of surface roughness and oxidation on *pool boiling*, a systematic investigation of the effect of micro-structural change (surface morphology, coating thickness, porosity, pore size, specific surface area) and wettability change due to surface oxidation and nano-coating (using nanoparticles) used with porous-layer structured surface on *falling-film evaporation* is not believed to exist.

[34] The capillary-assisted (gravity-insensitive) liquid distribution using the disclosed porous integral fins with nano-coating for surface wettability can be useful in various cooling devices, such as falling-film, horizontal-tube evaporators, where the liquid maldistribution, poor surface wetting and localized liquid droplet inherently tends to occur.

[35] Porous-layer coatings on a copper substrate were used to characterize the effect of the wick parameters on boiling performance. Figure 1(a) shows the boiling test apparatus under saturation (closed) conditions. Figure 1(b) shows a sintered

copper wick (1 inch in diameter and 1mm thick) tested with water for the boiling test. The wick was not completely immersed in water, but rather horizontally positioned slightly (~1mm) higher than the water level so that water was radially drawn from the side wall of the wick toward the center by capillary pumping. Considering the wicking distance (0.5 inches) and heat flux level (~100W/cm²) of the boiling tests, the wicking (capillary-assisted liquid distribution) and high heat flux evaporation using the disclosed porous integral fins (1 inch in height) is achievable. From the bubbling pressure measurement using a test sample with water (about 8,718 Pa), the pore diameter of the wick sample is estimated to be about 17μm. The heat flux measurement results using the fully-oxidized copper wick (as shown in Figure 1(b)) were in reasonable agreement with the results using another wick design and similar boiling conditions.

[36] Flow Mode and Surface Wetting Experiment using Falling-Film Water on Horizontal Copper Tubes

[37] The results of a preliminary study was conducted to investigate the effect of a porous-layer coating of horizontal tubes on surface wetting using falling-film liquid flow. Figure 2 shows the flow modes and surface wetting for falling-film water on two-row horizontal copper tubes with (a) plain surface and (b) porous-layer coating at various liquid Reynolds numbers ($\mathrm{Re}_{liq} = 4\Gamma/\mu_{liq}$). ζ is the surface wetting ratio defined as $\zeta = A_{wet}/A_{tube,outer}$. It was observed from the figure that the flow mode between the evaporator tubes [top (second row) and bottom (third row) tubes] was changed from the droplet to the droplet/column mode at the lower Reynolds number than the transitional Reynolds number (Re_{liq} = 352) known for plain tubes. The early flow mode transition might attribute to the liquid dispenser

design such as hole interval and diameter used for this experiment. Note that the flow mode between the liquid dispenser and the top tube is quite different than one between the top and bottom tubes. The surface wetting ratio (ζ) for the plain tubes as shown in Figure 2(a) was determined by counting the unwetted areas from the photo images. As shown in the figure, there was significant unwetted area on the plain tubes and the wet area was increased as the liquid Reynolds number was increased. On the contrary, there was observed no unwetted area on the porous-layer coating tubes as shown in Figure 2(b). The *complete* wetting on the porous-layer coating tubes was confirmed by touching the tube with a dry paper tissue at various locations and finding the paper wet even at the lowest liquid Reynolds number of 6.1.

[38] Contact Angle Measurement of Oxidized Copper

[39] Contact angle measurement is often used to measure the affinity of a liquid with surfaces. Figure 3 shows computer images of the contact angle measurement. As an attempt to confirm the well-known hydrophilic property of the metal oxides (copper (I) oxide), a contact angle measurement was performed using an optical contact angle and surface tension meter (model: CAM-100, manufacturer: KSV) based on the sessile drop method equipped with a high speed digital camera and an image analyzing software. Distilled water was used as the testing liquid. For the contact angle measurement, six test coupons (W×L=25mm×15.2mm) made of Oxygen Free High thermal conductivity Copper (OFHC) were prepared. Each coupon was prepared by first polished (only in one direction) by a very fine sandpaper (1500 grit), deoxidized with a commercial cleaner (TARN-X), dried, and then rinsed with acetone. Note that water and copper is chemically compatible and

the copper oxidation is mainly affected by oxygen concentration in environment and accelerated at elevated temperatures.

[40] For mild oxidation, two test coupons (samples #4 and 5) were left for two days in open air. Note that in Reno NV, where the tests were performed, the air is dry (~45% humidity) and the atmospheric pressure is about 0.89 atm. Another test coupon (sample #6) was heated at 100°C for 2 hours on an electrical hot plate to accelerate the oxidation in open air. All the samples were tested within 5~10 minutes after the sample preparation.

[41] The contact angle measurement results are also listed in Table 1. The polished surfaces (oxidation-free, Figure 3(a)) have the contact angles between a range of 75°~80°, whereas the surfaces oxidized at 100°C for two hours (accelerated oxidation, Figure 3(c)) show a significantly decreased contact angle of 62.78°. However, the results show that the oxidized samples (Figure 3(b)) at room temperature for two days have a negligible change in the contact angle from those of the polished surfaces. The contact angle measurement results support that aging (oxidation) improves surface wettability (hydrophilicity) and oxidation temperature plays a role in the oxidation level. It implies that monitoring of the aging effect may be beneficial because an improper aging procedure can cause inconsistent results for two-phase heat transfer experiments (boiling, condensation and evaporation).

[42] Typical boiling studies are performed in closed systems after degassing of noncondensible gases (e.g., air) which could be intentionally or accidentally introduced during a series of assembling and liquid charging or already exist in working fluids as a dissolved gas. Note that air contains oxygen (20.9% vol). The aging (oxidation) is mainly affected by an exposure time of metal samples to

oxygen, its concentration and temperature. The detailed oxidation mechanism is discussed below. After degassing, the low concentration air (or oxygen) in the systems could cause a slow oxidation. By measuring oxygen concentration in the system, the aging can be systematically monitored and controlled for consistent and time-efficient boiling studies. It is common to observe that most of open literatures on two-phase experimental works loosely use the aging term to explain the conditions used in their experiments. The present disclosure establishes a rigorous testing protocol for the two-phase experiments which are greatly affected by oxidation (aging).

[43] Table 1 Surface contact angle measurement results

Polished (*Oxidation-Free*) Surfaces (using Grit 1500)			*Mild* Oxidation Surfaces (at room temperature for two days in ambient)		*Accelerated* Oxidation Surface (at 100°C for two hours in ambient)
Sample-1	Sample-2	Sample-3	Sample-4	Sample-5	**Sample-6**
75.43°	78.25°	79.57°	72.97°	82.39°	**62.78°**

[44] One aspect of the present disclosure is to provide capillary-assisted evaporation in nano-coating, porous integral fins on falling-film, horizontal-tube evaporators. The same capillary (gravity-insensitive) liquid distribution, and consequently, thin film evaporation (low thermal resistance of 0.05K-cm²/W) used in wicked heat pipes can be used to mitigate inherent liquid maldistribution and surface nonwetting problems of the conventional plain surface evaporators and create an ideal evaporation condition, i.e., thin film evaporation with low-thermal resistance over increased surface wetting even with less supply of liquid. The disclosed porous integral fins can further enhance the evaporation due to the increased evaporation area.

[45] The present disclosure allows the effects of the following variables/conditions to be used to enhance falling-film evaporation: physical variables (porosity, permeability, pore size (10~100μm), pore size/distribution, and specific surface area) and geometrical properties (fin height (~1cm), width and pitch), thermo-physical properties (effective thermal conductivity) of porous integral fins and surface wettability (nano-coating), evaporator design (tube diameter/length/spacing and liquid dispenser) and operating conditions (flow rate and temperature of feed liquid and vapor pressure).

[46] Porous Integral Fin Fabrication

[47] The present disclosure, in one specific embodiment, uses sintered (diffusion bonded) powders (e.g., copper and metal oxides) to create porous coating/integral fins using physical properties of porous media (porosity, permeability, pore size/distribution, and specific surface area), geometrical variables of porous integral fins (fin pitch, height, and thickness; fin base thickness) and evaporator design variables (tube diameter, length, number of tubes and nozzle height). In some implementations, sintering techniques for sintered metallic (copper, and nickel) powder/screen composite for two-phase heat sinks (e.g., heat pipes) for high performance electronic cooling can be applied to achieve the disclosed purposes.

[48] In one example, the porous integral fins made of metal powder and/or screen meshes are built on a substrate by diffusion bonding (sintering) in a mold using a multi-step procedure. A rendering showing the multi-step sintering process is illustrated in Figure 4. The molds (stainless steel or graphite), in a more specific example, are fabricated to provide a 3-D negative image of desired surface structures on the substrate. The dimensions of the porous structures can be chosen as desired

can be determined, for example, by the fabrication method and machining tolerance of the molds.

[49] The process, in a particular example, proceeds as follows. First, the metal powders are filled into a mold through fill ports and are shaken compact. Then, the powder-laden molds are placed into a high temperature, quartz glass tube furnace and heated up to sintering temperatures (≤1000°C for copper powder), which is lower than melting temperature of the metal, in an inert/reducing atmosphere such as a nitrogen/hydrogen mixture (forming gas) over a preset time (< 1 hour for copper). At elevated sintering temperature, the metal particles are diffusion-bonded (sintered) to each other and to the copper substrate due to increased mobility of metal atoms creating a desired 3-D porous structure. The sintering duration can vary with metal powder kind, particle size, surface condition and size of sintering sample. Particles with nominal diameters as small as 50 μm are considered suitable for sintering.

[50] This sintering technique has been used, for example, for fabrication of micro-scale pore structures used for heat pipes. Other fabrication methods can be used, such as for higher production rates for the modulated coatings. The surface morphology of the micro-scale porous coating can be visually inspected and or measured using suitable techniques, such as SEM and AFM.

[51] Figure 5(a) shows a porous integral fin illustrating a capillary-driven liquid flow/distribution and surface evaporation of the liquid drip from a liquid dispenser. The porous layer adjacent to the heating substrate provides liquid flow conduits to fins built on the substrate. The geometric optimization of the porous fins (spacing (pitch), height, thickness, and shape) allows for low pressure drops for liquid flow. Figure 5(b) shows a porous integral fin fabricated using a sintering furnace.

[52] Falling-Film Evaporation

[53] To verify the enhancement mechanism of falling-film evaporation using the porous integral fins, the porous integral fins (as shown in Figure 5 as an illustrative example) of sintered metal powder on horizontal tubes are tested in a hermetically-sealed chamber under saturated or reduced pressure conditions. A plain tube evaporator is tested to establish the baseline results of evaporation heat transfer coefficient and liquid distribution/wettability and number of droplet sites. To establish a validity of the evaporation studies, the baseline results are compared with published data based on the same conditions.

[54] A schematic of an example of a hardware setup for falling-film evaporation is shown in Figure 6. The hardware setup based on a closed-system design consists of at least three basic components: (i) an evaporator with a heater/degassing system; (ii) a condenser with a chiller system in a hermetically-sealed chamber with a vacuum pump; and (iii) a measurement/control system. Some evaporation methods are carried out using high surface tension fluids (e.g., water) and low surface tension fluids (e.g., refrigerants) as the working fluids. In a specific example, the evaporation chamber is constructed of a corrosion-resistant stainless steel (SS 316) which is compatible to the working fluids and be designed to endure high pressures for the vapor pressure of the working fluids. The wet components (e.g., gasket, valve and fitting) are typically chosen depending on the material compatibility level with the working fluids.

[55] A quartz glass viewport in the chamber can be used to view and record the falling-film evaporation and surface wetting condition on the horizontal tubes using a long-focal point microscope/high speed video camera and an infrared thermometer

camera. The visual observation using the high speed camera can provide information on liquid film/droplet distribution on the tube surface and liquid drip pattern in the tube bundle. The infrared thermal image can provide an accurate estimation of the wetted surface area by measuring a sharp change in the surface temperature distribution due to surface evaporation. The infrared thermal image may also be used to measure the surface temperature distribution for evaporation heat transfer calculation, in addition to the direct temperature measurement using thermocouples embedded in the evaporator tubes.

[56] In some methods, the working liquid is degassed before use using a heater/degassing tank with an ultrasonic stirrer as shown on the left side of Figure 6. Such a system can, with, for example, FC-72. Fluorocarbons can absorb a significant degassing of air at atmospheric conditions. Depending on the loop construction, this separate degassing system might be omitted, in some examples, such as for water, and sufficient degassing could be obtained by running the evaporation/boiling loop for a significant time before official operation (this would separate any dissolved gases in the system) and evacuating the collected gases from the upper part of the chamber using a vacuum pump. Degassing helps control the evaporation/condensation affected by non-condensable gases and if air exists in the system, surface oxidation of evaporator tubes would alter the evaporation performance over time.

[57] A temperature-controlled, external cooling/heating loop is used, in some examples, to control the temperatures of the evaporator and condenser. The evaporator may be heated by a heating fluid circulated by an external heating loop. The condenser may be cooled by a coolant loop connected to an external chiller

loop. The system can be insulated with commercial insulation materials. This helps to provide quicker heating/cooling to reach a steady-state condition. A series of copper-constantan (T-type) thermocouples can be embedded along the evaporator tubes (axially and circumferentially). The evaporation heat transfer rate may be estimated using the measured temperature differential of the heating fluid at the inlet and outlet of the evaporator tubes. Similarly for the condenser heat transfer measurement. Evaporation studies can be performed to generate heat transfer coefficient curves by gradually varying wall superheat of the evaporator and ambient pressure (by varying condenser temperature).

[58] When a liquid film flows from one horizontal tube to another below it, according to an increasing flow rate order, the flow may take the form of droplets, circular jets or continuous sheet.

[59] Both porous integral fins (tube diameter, fin height, width, pitch) and porous medium properties (porosity, permeability, specific surface area, pore size/distribution, and effective thermal conductivity) can be optimized for improved system performance.

[60] Surface Oxidation Kinetics

[61] The oxidation layer thickness ( ) of metals under a high temperature oxidizer can be generally estimated by the following exponential oxidation law

[62] $$d = \sqrt{2k_o \exp\left(\frac{-Q_o}{RT}\right)t} \qquad (1)$$

[63] where k_o is the oxidation constant [m^2/s] and Q_o is the activation energy [J/mol] and T is the oxidation temperature [K] and t is the elapsed time [sec]. k_o and Q_o are empirically determined. For a steel (grade: MS1200), k_o=0.076 m^2/s and Q_o

=239 kJ/mol. The effect of oxygen concentration is not considered in the above equation. The oxygen concentration, along with the metal specimen temperature, can affect the oxidation rate. If oxidation occurs in a closed system under saturation or reduced pressure (i.e., very low oxygen concentration), the oxidation rate is typically slower than under ambient condition (20.9% vol. oxygen). Since the oxidation layers increase the thermal resistance of the conduction heat transfer because of low thermal conductivity than the fresh surface, the thickness of the oxidation layer may influence heat transfer reduction.

[64] Nano-Scale Surface Morphology of Oxidation Layer

[65] Copper is often used for boiling surfaces because of its high thermal conductivity and good chemical compatibility with many working fluids, including water. But copper becomes easily oxidized forming copper oxides (Cu_2O and CuO) even at room temperature while exposed to oxygen in air while preparing samples The reddish copper oxidation (copper (I) or cuprous oxide, Cu_2O) is naturally formed in ambient conditions over an extended time. Accelerated formation of the surface oxidation is usually achieved at elevated temperatures. With further heating, the copper (I) oxide is converted into a blackish copper oxide (copper (II) or cupric oxide, CuO).

[66] Since many applications, such as heat pipes, are closed systems, the oxidation can be significantly reduced, but not completely removed, depending on preparation conditions and assembling procedure.

[67] Surface morphology changes due to surface oxidation can be characterized by AFM and/or SEM using test coupons oxidized under various temperature and oxygen-concentration over different oxygen-exposure times and quantitatively

measured in terms of coverage area and thickness of the oxidation layer, and the effect of the oxidation level on thin falling-film evaporation investigated by the contact angle measurement. To quantitatively measure the change of the surface morphology due to surface oxidation, test coupons free of oxidation can be prepared (cleaned in a tube furnace using a reducing environment or chemically) as a baseline surface condition and used for surface roughness measurement using AFM in an environmental chamber or a glove box using temperature-controlled and inert cover gases (e.g., Ar or N2).

[68] To quantitatively measure the increase of surface wettability due to the surface oxidation, the contact angle measurement can be performed in the environmental chamber to establish a correlation between the contact angle and surface morphology measurements. To preserve the samples from being further oxidized before being used for evaporation experiments, a protective cover and/or coating can be used. This approach can provide more repeatable and consistent study on the in-situ surface oxidation.

[69] Nano-Coating for Surface Wettability Control

[70] In addition to surface oxidation, surface nano-coating is an effective way to create various surface wettability from hydrophilicity (SiO_x, TiO_2, Pt and Fe_2O_3) to hydrophobicity (SiOC and Teflon). Particles of very small size (typically less than 100 nm) called "nanoparticles" can be deposited, such as on heated surface using Metal-Organic Chemical Vapor Deposition (MOCVD) and Plasma Enhanced Chemical Vapor Deposition (PECVD) and Nanofluid Nucleate Boiling Deposition (NNBD). Nanofluids that include metal oxide nanoparticles, such as Alumina (Al_2O_3), Zirconia (Z_rO_2) and Silica (SiO_2), for pool boiling indicate that the boiling

critical heat flux increases significantly as compared to those of the pure fluids. The enhanced heat flux is likely at least partially due to increased surface wettability of the nanofluids by deposition of the nanoparticles on the heater surface. In this disclosure, the effect of the micro-structural variables such as porosity, pore size, and specific surface area of nano-coating on the wetting property are used to enhance cooling devices. In some examples, oxide materials such as Alumina, Zirconia, Silica, and Titania (TiO2) are used for nano-coatings.

[71] Tailoring surface nano-coatings to create specific wetting properties the surface wettability level to be correlated to evaporation performance. Nano-coatings also allow surface wettability to be modified without significant changing the micro/macro-scale surface topology of the porous structured surfaces.

[72] Design of Falling-Film Evaporation in Porous Media

[73] Theoretical considerations can be used to predict and identify dry-out, maximum heat flux of conditions the falling-film evaporation using porous media. Theoretical analyses, in one example, are a combination of analytical and numerical solutions to the governing equations for two-phase flow and heat transfer in plain and porous media. Numerical solutions based on the finite-volume can be performed on the plain and porous media governing equations. The overall goal is to apply the theory of the evaporation in structured porous layer (as shown in Figure 5 as an illustrative example). This information can be used to enhance the design of the capillary-driven evaporator systems.

[74] Falling-Film Evaporation

[75] The falling liquid flow around a smooth, horizontal tube can be divided into four regions: stagnation, Jet impingement, thermal developing and fully-developed.

The jet impingement region has the largest heat transfer coefficient due to a small surface-convection resistance of jet impingement flow. The stagnation region is often a very small portion of the circumference of the tube and is often neglected for heat transfer calculation. In the thermal developing region, a thermal boundary layer typically develops, resulting in a large thermal resistance. Thinning the liquid layer in the thermal developing and fully developed regions can enhance the overall evaporation performance.

[76] Using porous fins on evaporators can allow for less liquid flow, creating a favorable thin liquid film layer resulting in enhanced evaporation. The heat transfer can be reduced at the jet impingement region due to the slow liquid flow but increased for the rest of the regions because of thinner film evaporation.

[77] The non-boiling heat transfer coefficient for smooth horizontal tubes is given by

[78] $$\bar{h}\left(\frac{\nu^2}{gk^3}\right) = C\,\mathrm{Re}^{0.15}\,\mathrm{Pr}^{0.53} \qquad (2)$$

[79] where $\bar{h}$ is the averaged heat transfer coefficient and C is the constant varying with the tube diameter and k is the thermal conductivity of the liquid film. The disclosed porous structured coating made of metallic materials (e.g., copper) provides a higher effective thermal conductivity than that of the liquid film and the constant C can increase due to surface wettability increase by the surface oxidation and nano-coating. As a result, higher evaporation heat transfer coefficients may be achieved.

[80] Spreading of Liquid Drops in Porous Layers

[81] Spreading of liquid drops over thin porous layers (which are saturated with the same liquid) is a phenomena useable to understanding the liquid distribution in the disclosed porous integral fins and the falling-film evaporation. The spreading of the liquid drops over the porous media is governed by the same power law as in the case of spreading over a dry solid substrate. The evolution of the drop profile can be calculated by integrating the Navier-Stokes equations with boundary conditions considering a slippage condition over the porous layer. The following Brinkman's equation can be used to model the liquid flow inside the porous layer and slippage velocities for the calculation of the evolution of the drop profile.

[82] $$0 = -\nabla P_l - \frac{\mu}{K} u_l + \mu_e \nabla^2 \langle u_l \rangle \qquad (3)$$

[83] Evaporation under Reduced (Vacuum) Pressures

[84] Evaporation under reduced (vacuum) pressures, which is lower than the saturated pressure, requires non-equilibrium treatment for the phase change. For an evaporation process according to the present disclosure, the pressure of the vapor at the liquid surface (P_{vap}) could be less than the saturation vapor pressure (P_{sat}) corresponding to the liquid surface temperature (T_{sat}). From a kinetic theory of phase change under such low pressures, the evaporation rate can be calculated by

[85] $$\dot{m}'' = \frac{2\sigma}{2-\sigma}\left[\frac{P_{sat}}{(2\pi R T_{sat})^{1/2}} - \frac{P_{vap}}{(2\pi R T_{vap})^{1/2}}\right] \qquad (4)$$

[86] where ← 1 is used for water vapor molecules at non-contaminated surface. The evaporation heat flux is calculated by $q_{eva} = \dot{m}'' h_{fg}$.

[87] Two-Phase Heat Transfer Modes in Porous Media

[88] Two-phase heat transfer (evaporation and boiling) in porous media is typically more complex than from plain surfaces due to the existence of porous structures. The heat transfer, liquid film distribution and vapor formation may change with porous media properties (material and geometrical), operating conditions and working fluids. As a result, four major operation modes determined by the "heat flux or wall superheat" may exist in the evaporation/boiling and are shown schematically in Figures 7A-7D based on an uniform plain porous layer to help discussion in next sections.

[89] (i) Conduction-Convection-Surface Evaporation

[90] As shown in Figure 7(A), at the low heat flux conditions, the entire porous layer is fully saturated with liquid where conduction occurs across the liquid layer and evaporation takes place from only the surface (liquid-vapor interface) of the porous layer. The heat transfer across the porous layer can be calculated by a conduction model. No boiling occurs within the porous layer. Natural convection may occur within the porous layer under a gravitational field. The heat transfer across the wick can be calculated by a conduction mode given by:

[91] $$q/(T_s - T_v) = \langle k \rangle_{wick} / L_k \qquad (5)$$

[92] $\langle k \rangle_{wick}$ is the effective thermal conductivity of the porous layer. L_k is the thickness of the wick and calculated based on the averaged thickness of the 3-D structured wick. The flow and pressure drop through porous media can be modeled using the following Darcy-Ergun equation:

[93] $$0 = -\nabla P_l + \rho_l g - \frac{\mu}{K}\langle u_l \rangle - \frac{C_E}{K^{1/2}}\rho_l |\langle u_l \rangle| \langle u_l \rangle \qquad (6)$$

[94] The capillary pressure ($\Delta P_{c,\max} > \Delta P_l$) can be related to the liquid saturation, porosity, permeability and wettability using Leverett J-function.

[95] (ii) Conduction-Convection-Surface Evaporation

[96] As shown in Figure 7(B), as heat flux is gradually increased, the evaporation at the liquid surface intensifies. The capillary pumping may not be large enough to feed liquid. Consequently, the liquid begins to recede into the porous layer. If the receding of liquid continues, the liquid at the evaporator may completely dried out. This limit encountered is called as the "capillary (or hydrodynamic) limit" (not the boiling limit). Before the liquid is completely depleted, the heat transfer across the liquid layer is still by conduction, and the liquid vaporization takes place at the liquid-vapor interface. No boiling occurs within the porous layer.

[97] (iii) Nucleate Boiling

[98] As shown in Figure 7(C), when the heat flux further increase and therefore the temperature difference (wall superheat) across the wick becomes large, nucleate boiling may take place within the porous layer. Bubbles grow from the nucleate boiling sites in the porous layer, escape to the liquid surface and burst rapidly. Since the liquid feed in the porous layer is driven by the capillary force, nucleate boiling in the porous layer represents a heat transfer limit (boiling limit).

[99] (iv) Film Boiling

[100] As shown in Figure 7(D), as the temperature difference across the porous layer is further increased, a large quantity of bubbles is generated at the heating surface. These bubbles coalesce together, forming a blanket of vapor adjacent to the heating surface, which blocks the liquid from reaching the heating surface. This heat transfer limit is called as the "boiling limit" which is similar to the critical heat

flux condition in pool boiling, and is the maximum heat transfer limit for the film boiling for the following reasons: (1) large bubbles bursting may destroy the menisci at the liquid-vapor interface and interrupt the capillary-driven liquid flow; and (2) vapor bubbles formed in the evaporator porous layer may hinder the liquid flow. The boiling limit is similar to the critical heat flux condition in pool boiling, and is the maximum heat transfer limit for the boiling in the porous layer.

[101] The disclosed falling-film evaporator, in one implementation, uses low heat fluxes (or low superheats) conditions to create the surface evaporation condition (as shown in Figures 7 (A) and (B)) and to limit the nucleate boiling at high heat fluxes in porous media. The reduced pressure conditions will be also used to promote the surface evaporation using sub-cooled liquid.

[102] It is to be understood that the above discussion provides a detailed description of various embodiments. The above descriptions will enable those skilled in the art to make many departures from the particular examples described above to provide apparatuses constructed in accordance with the present disclosure. The embodiments are illustrative, and not intended to limit the scope of the present disclosure. The scope of the present disclosure is rather to be determined by the scope of the claims as issued and equivalents thereto.

What is claimed is:

1. An apparatus comprising a plurality of nano-coated, porous integral fins and/or grooves on the evaporator tubes.

2. The apparatus of claim 1, wherein the apparatus is an evaporative cooler.

3. The apparatus of claim 1, wherein the apparatus is a horizontal-tube, falling-film evaporator.

4. The apparatus of claim 1, wherein the evaporator tubes are in either horizontal and/or tilted and/or vertical position.

5. The apparatus of claim 1, wherein one or more liquid dispensers are located either above and/or below the evaporator tubes.

6. A method of using the apparatus of claim 1 as a cooling device.

7. A method of using the apparatus of claim 1 as an evaporative cooler.

8. A method of using the apparatus of claim 1 as a falling-film evaporative cooler.

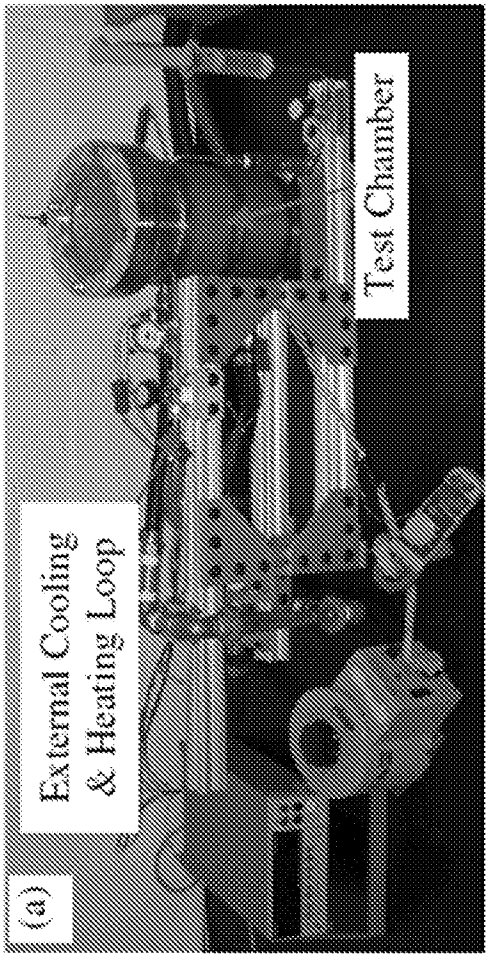
(a)
External Cooling & Heating Loop
Test Chamber

FIG. 1A

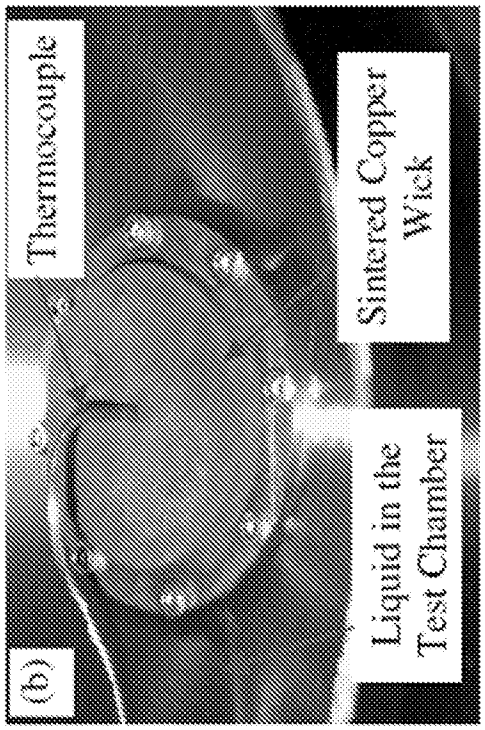
(b)
Thermocouple
Sintered Copper Wick
Liquid in the Test Chamber

FIG. 1B

FIG. 2A

FIG. 2B

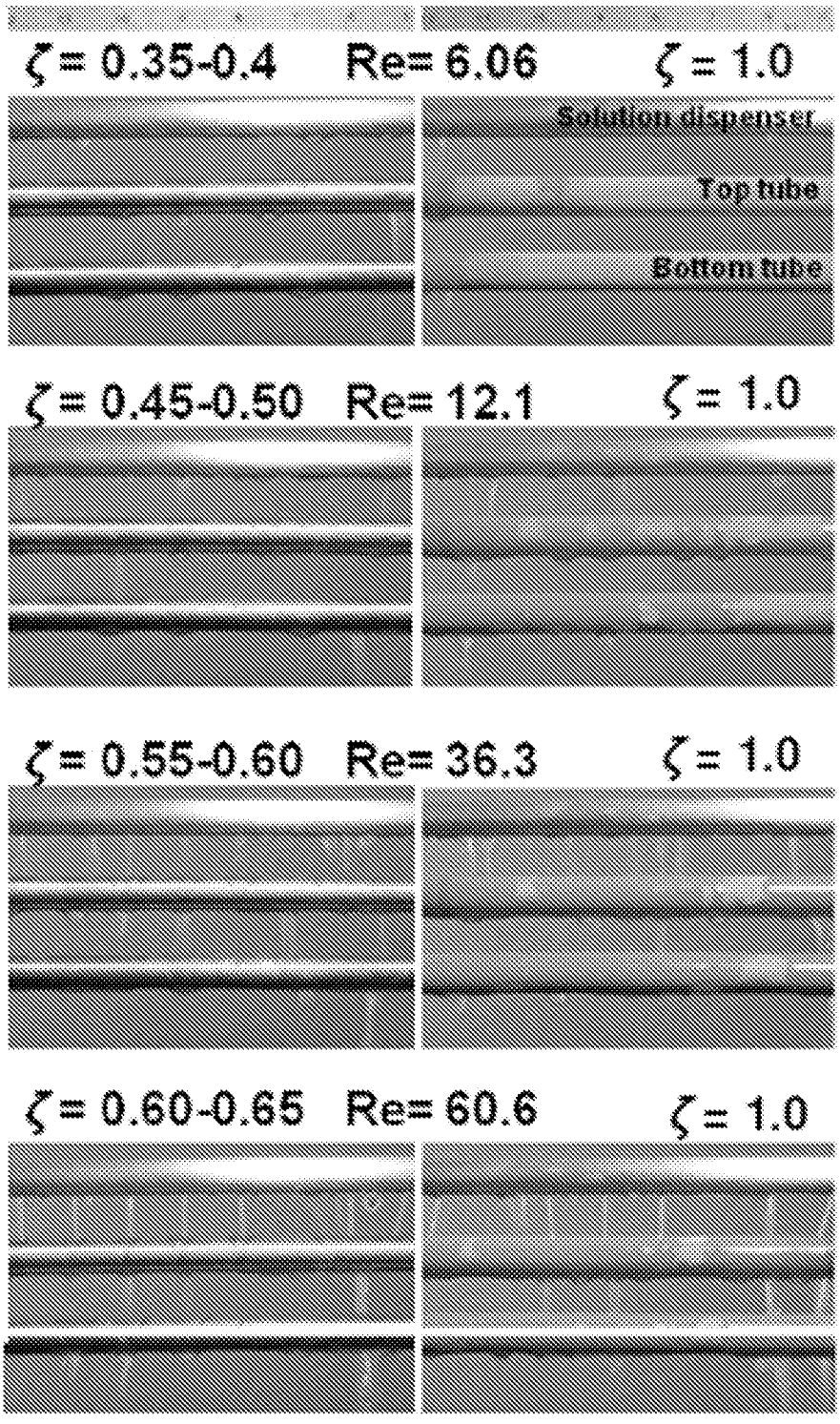
ζ = 0.35-0.4
Re= 6.06
ζ = 1.0
Solution dispenser
Top tube
Bottom tube
ζ = 0.45-0.50
Re= 12.1
ζ = 1.0
ζ = 0.55-0.60
Re= 36.3
ζ = 1.0
ζ = 0.60-0.65
Re= 60.6
ζ = 1.0

FIG. 3A

FIG. 3B

FIG. 3C

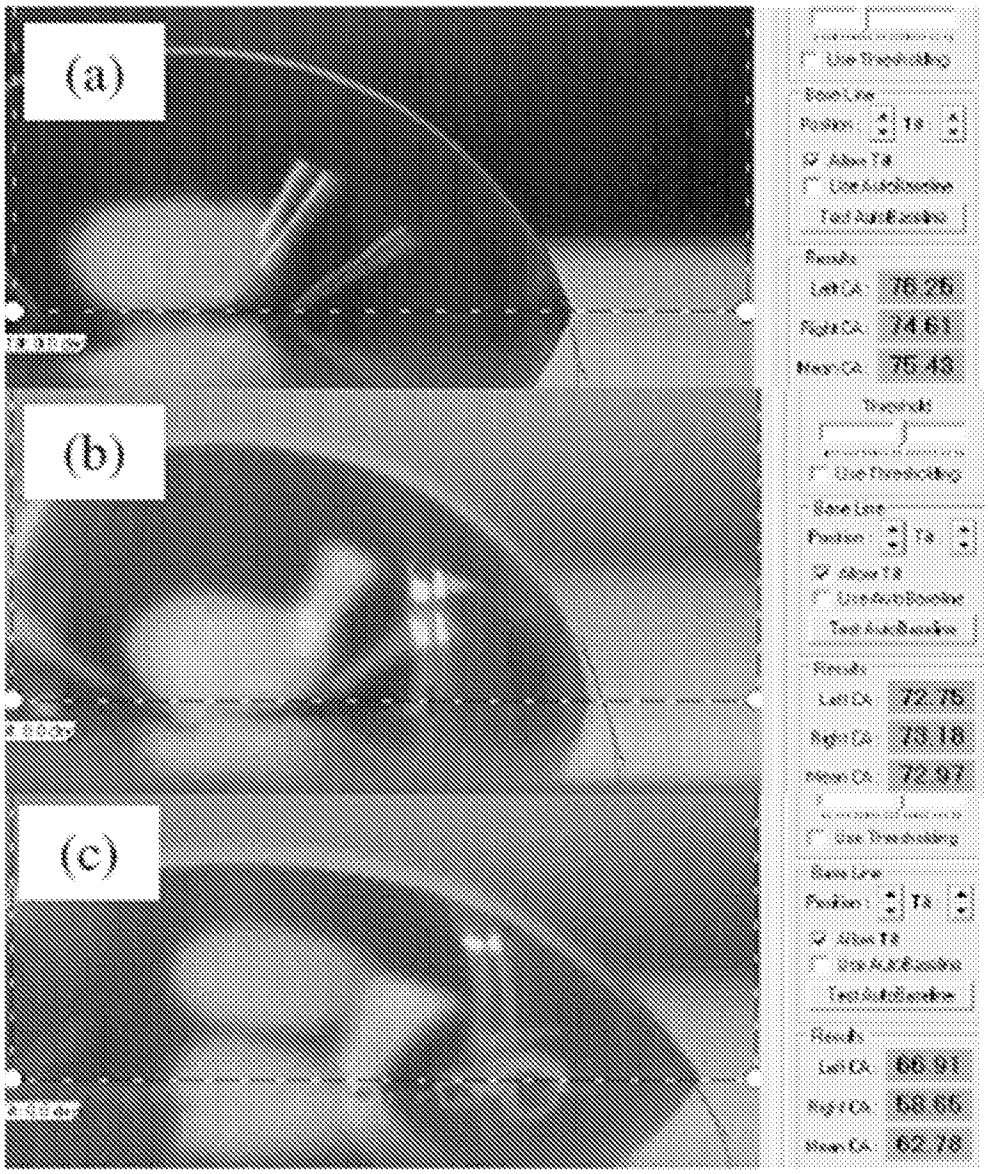

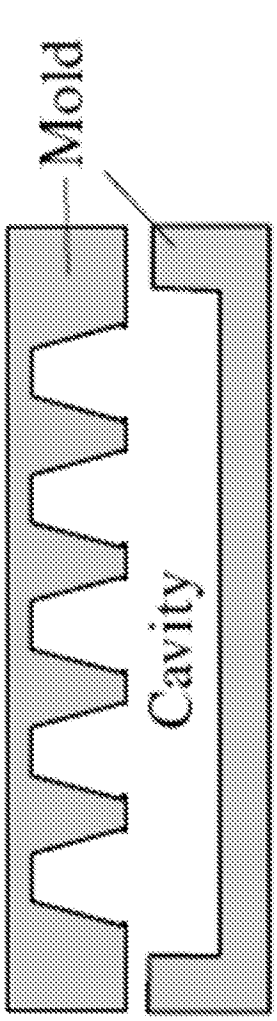

FIG. 4A

Machining a mold with an open cavity

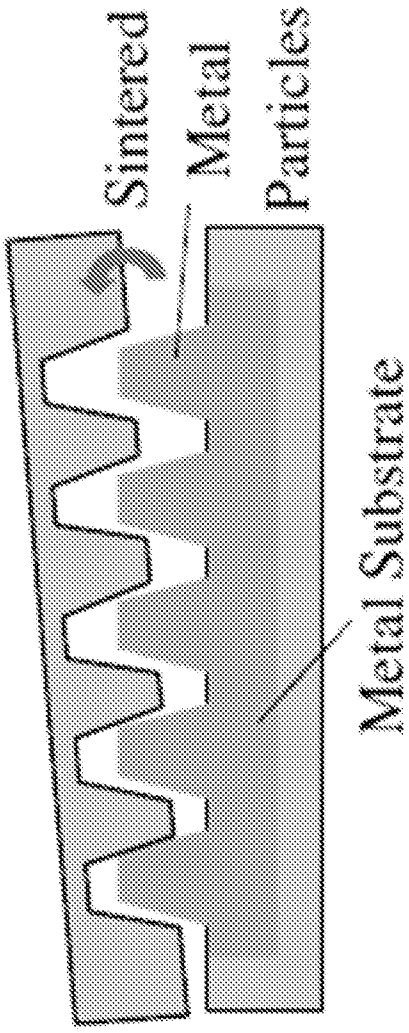

FIG. 4B

Filling metal powder into the mold and sintering onto the metal substrate.

FIG. 5A

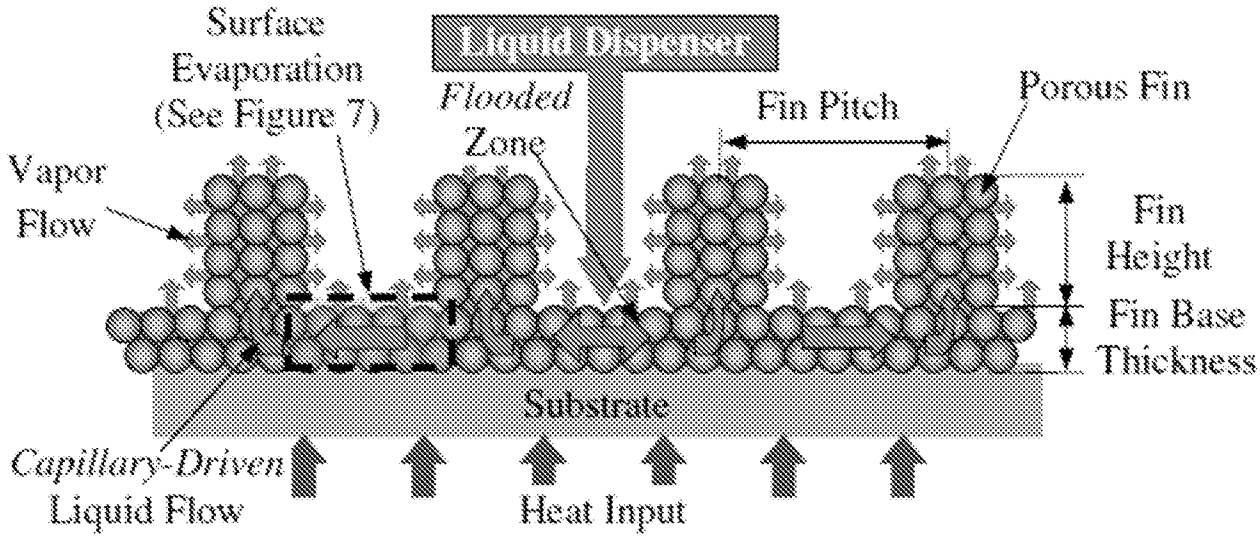
Surface
Evaporation
(See Figure 7)
Liquid Dispenser
Flooded
Zone
Fin Pitch
Porous Fin
Vapor
Flow
Fin
Height
Fin Base
Thickness
Substrate
Capillary-Driven
Liquid Flow
Heat Input

FIG. 5B

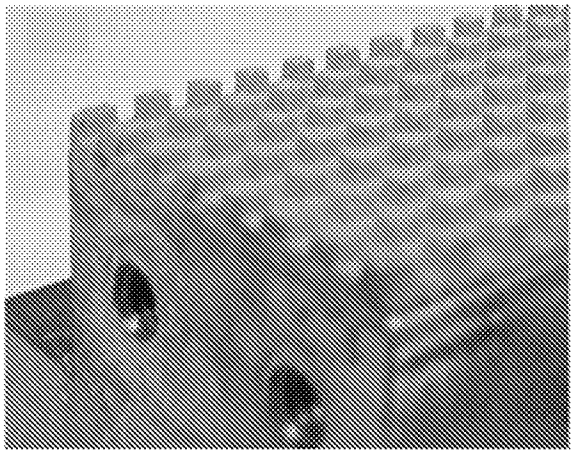

FIG. 5C

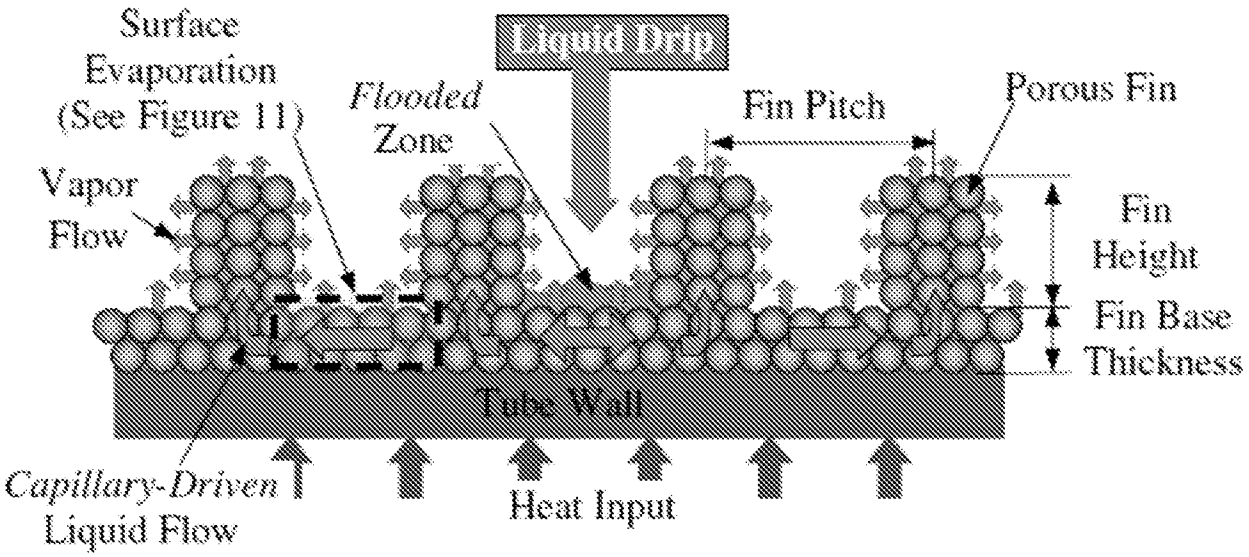
Surface Evaporation (See Figure 11)
Liquid Drip
Flooded Zone
Fin Pitch
Porous Fin
Vapor Flow
Fin Height
Fin Base Thickness
Tube Wall
Capillary-Driven Liquid Flow
Heat Input

FIG. 5D

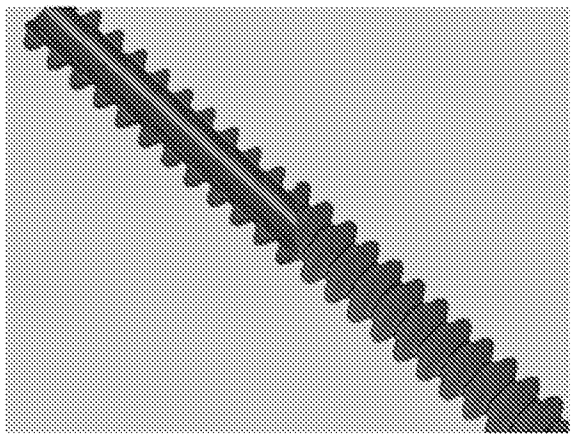

FIG. 6

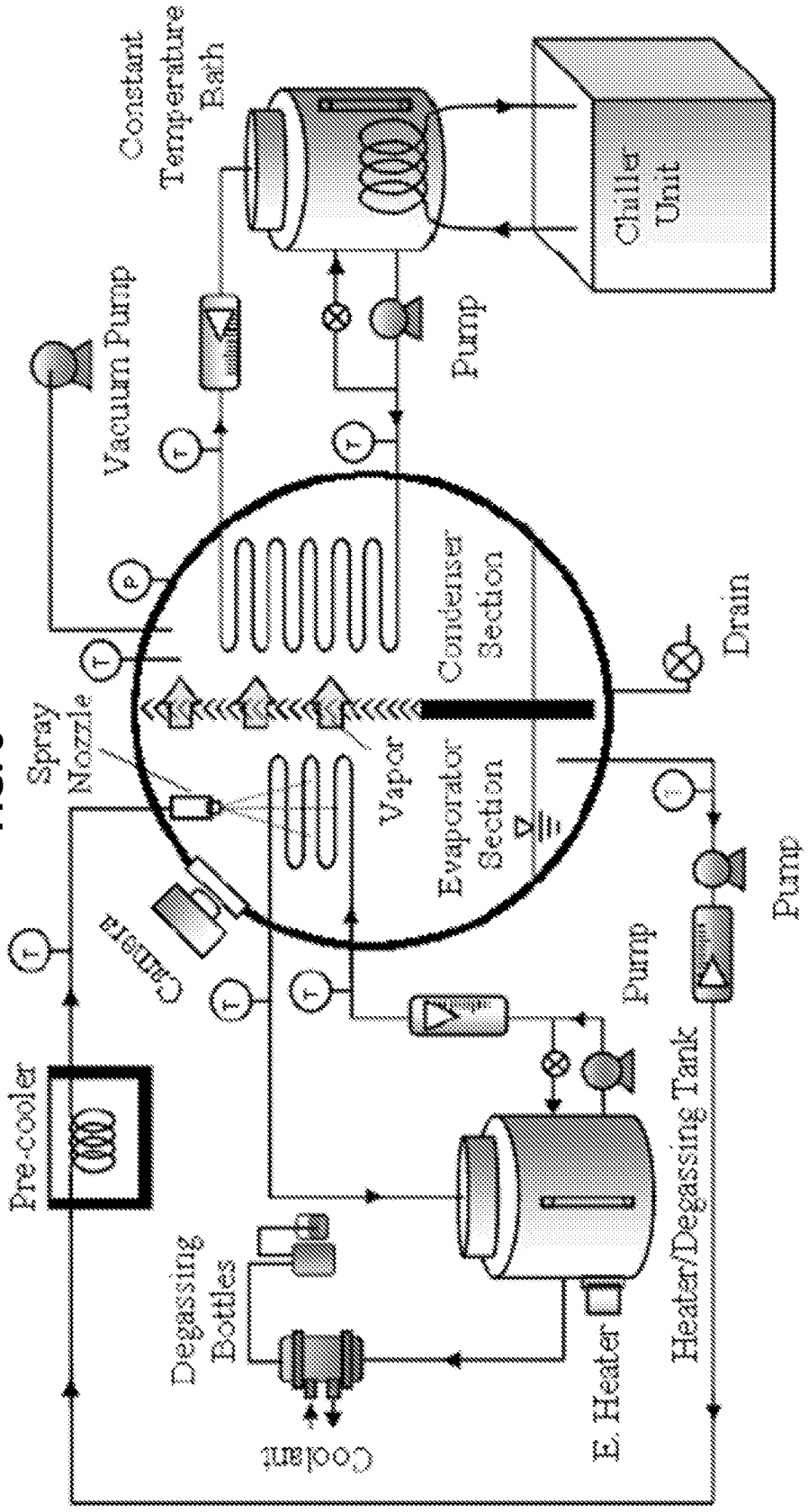
Constant Temperature Bath
Chiller Unit
Vacuum Pump
Pump
Condenser Section
Drain
Spray Nozzle
Vapor
Evaporator Section
Camera
Pump
Pump
Pre-cooler
Degassing Bottles
Heater/Degassing Tank
Coolant
E. Heater

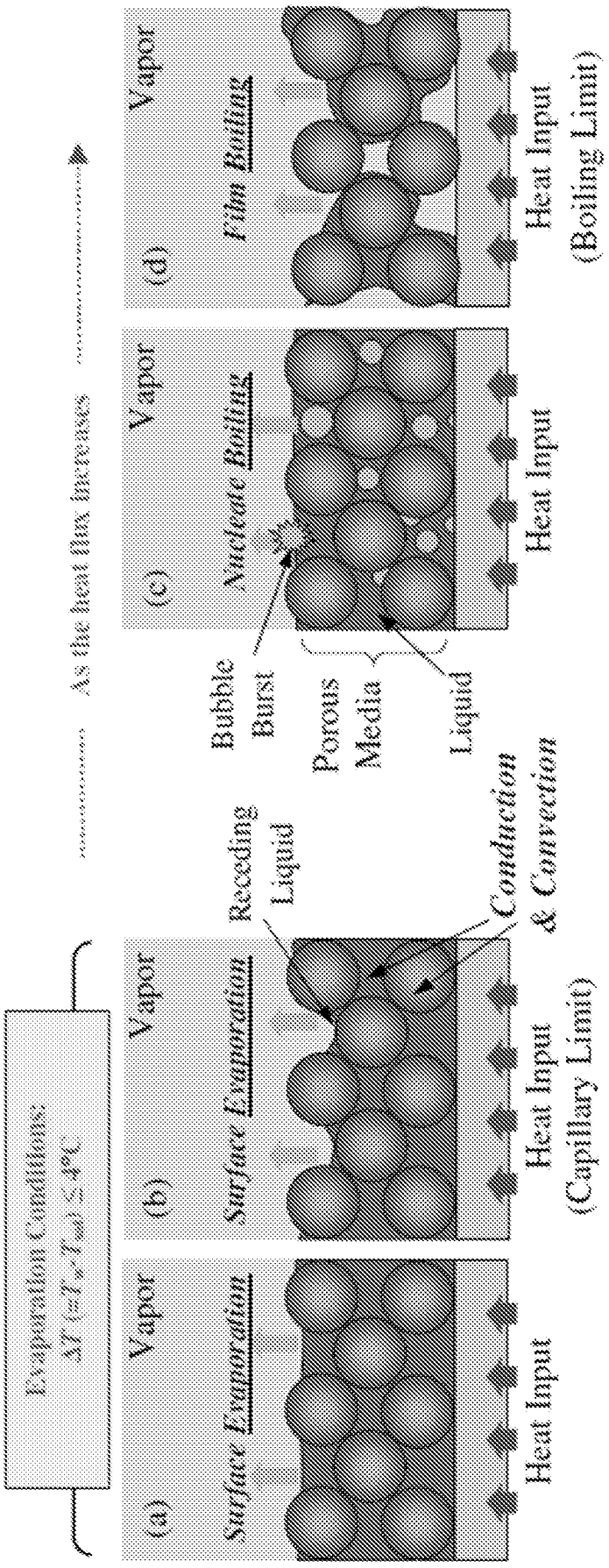
Evaporation Conditions:
$\Delta T (=T_w-T_{sat}) \leq 4°C$
As the heat flux increases
(a)
Surface Evaporation
Vapor
Heat Input
(b)
Surface Evaporation
Vapor
Receding Liquid
Conduction & Convection
Heat Input
(Capillary Limit)
(c)
Nucleate Boiling
Vapor
Bubble Burst
Porous Media
Liquid
Heat Input
(d)
Film Boiling
Vapor
Heat Input
(Boiling Limit)

FIG. 7